

# Automatic Estimation of the Corneal Limbus in Videokeratoscopy

Mark R. Morelande, D. Robert Iskander\*, *Member, IEEE*, Michael J. Collins, and Ross Franklin

**Abstract**—An algorithm for estimating the corneal limbus from videokeratographic images is proposed. After the image is transformed to a polar grid, a novel edge-detection procedure, suitable for the detection of the soft edge produced by the limbus, is used to locate the limbus. Outliers due to the eyelids, eyelashes, and videokeratographic rings are removed by taking advantage of the approximate circularity of the cornea. An ellipse which minimizes the sum of the squared algebraic errors is fitted to the remaining edge points. Comparisons between the proposed algorithm, a manual computer-based technique and an algorithm which uses conventional edge-detection techniques demonstrate the accuracy of the proposed algorithm.

**Index Terms**—Cornea, corneal centroid, soft-edge detection.

## I. INTRODUCTION

THE CORNEA is the major refracting component of the human eye, contributing approximately two-thirds of the eye's optical power [1]. The geometrical shape of the cornea predetermines, to a large extent, the optical characteristics of the eye. Aberrations such as astigmatism, coma and spherical aberration are often caused by deviations of the corneal surface from an idealized aspheric shape.

Videokeratoscopy is the current standard in accurate measurement of the shape of the corneal anterior surface [2], [3]. The majority of current videokeratoscopes are based on a placido disk approach [3]. The placido disk forms the target of rings, while a digital camera captures the reflected image from the tear film. The acquired image is processed so that the topographical corneal height can be calculated. The corneal height is usually measured relative to a reference plane or the best-fit sphere [4]. The radius of curvature or dioptric power can also be derived from the acquired image.

Complete measurement of the cornea requires three-dimensional (3-D) characterization, through modeling and analysis of corneal topography or dioptric power [5]–[9], and two-dimensional (2-D) characterization. A 2-D analysis, which will be the

subject of this paper, is primarily concerned with finding the position of the limbus. The limbus is the anatomical term for the perimeter of the cornea and is considered to lie at the transition from the cornea to the sclera. Once the limbus has been estimated important parameters such as the corneal centroid and diameter are easily found.

Knowledge of the corneal centroid is important when calculating the corneal surface area, or finding the difference between the location of the corneal apex (the point of greatest curvature) and the corneal centroid. For example, in human corneal transplantation it is of interest to measure the graft centration relative to the pupil center, corneal centroid, or the corneal apex [10], [11]. In contact lens fitting, on the other hand, the corneal apex and the centroid may influence the location of the lens on the eye [12]. Another application that is associated with corneal centroid location is the tracking of eye movements during refractive surgery [13].

Current videokeratoscopes provide a 3-D measurement of the corneal surface with the axis of the instrument corresponding to the corneal vertex normal. They also provide measurement of the pupil diameter but this information is often not reliable and highly dependent on the corneal surface itself, because the contour of the pupil may be obscured by the image of the placido disk rings. However, corneal limbus estimation is currently not implemented in videokeratoscopes. This causes vision researchers to rely on manual templates or basic morphological image processing algorithms applied to images taken with a separate digital camera [14], [15].

Thus, it is of interest to measure the 3-D surface of the cornea using a videokeratoscope and simultaneously provide a 2-D characterization of the cornea. The problem of obtaining a 2-D characterization of the cornea can be viewed as a problem of locating and estimating the corneal limbus. In turn, this can be put in a framework of edge detection, where the transition from the cornea to sclera is to be established. It is the purpose of this paper to provide a robust algorithm for solving this edge-detection problem. An adequate solution to this problem cannot be supplied by conventional image processing techniques due to the gradual nature of the transition from cornea to sclera and the presence of eyelids, eyelashes, and placido disk rings. It is therefore necessary to develop specialized techniques.

The paper is organized as follows. In Section II, we present an algorithm for accurately estimating the corneal limbus that overcomes all of the interferences present in placido disk-based videokeratographic images. Results are presented in Section III which confirm the validity of the proposed algorithm. Conclusions are drawn in Section IV.

Manuscript received December 12, 2001; revised July 16, 2002. *Asterisk indicates corresponding author.*

M. R. Morelande was with the Centre for Eye Research, Queensland University of Technology, Kelvin Grove Q4059, Australia. He is now with the Department of Electrical and Electronic Engineering, The University of Melbourne, Parkville VIC 3010 Australia.

\*D. R. Iskander is with the School of Engineering, Griffith University, PMB 50 Gold Coast Mail Centre, Q9726, Australia (e-mail: r.iskander@mailbox.gu.edu.au).

M. J. Collins and R. Franklin are with the Centre for Eye Research, Queensland University of Technology, Kelvin Grove Q4059, Australia.

Digital Object Identifier 10.1109/TBME.2002.805481

TABLE I  
SUMMARY OF THE ALGORITHM

1. Find the location of the corneal vertex normal.
2. Set the corneal centroid to the location of the vertex normal.
3. Perform the following several times:
(a) Construct a polar grid with radii $r_k$ , $k = 1, \dots, n_r$ and angles $\theta_l$ , $l = 1, \dots, n_\theta$ , where $n_r$ and $n_\theta$ correspond to the number of pixels in $r$ and $\theta$ directions.
(b) Transform the image from the Cartesian grid to the polar grid using the current centroid estimate.
(c) Estimate the position of the limbus for each $\theta_l$ , $l = 1, \dots, n_\theta$ .
(d)-(e) Remove edge points deemed to be outliers.
(f)-(g) Fit an ellipse to the remaining edge points to obtain an updated estimate of the corneal centroid, dimensions and orientation.

## II. CORNEAL LIMBUS ESTIMATION ALGORITHM

Our aim is to provide a 2-D characterization of the cornea from a gray-scale digital image of the eye obtained from a placido disk-based videokeratoscope. We denote the image intensity by  $h(x, y)$ ,  $x = 1, \dots, n_x$ ,  $y = 1, \dots, n_y$ , where  $n_x$  and  $n_y$  denote the number of pixels in the image in the  $x$  and  $y$  directions, respectively. We will refer to  $h(x, y)$  in short as a digital image.

The characterization procedure is complicated by the following factors:

- In many cases, the cornea is obstructed by the eyelids. In addition to preventing a full image of the cornea being obtained, the eyelids present a false edge. It is important to be able to distinguish between an edge presented by the eyelids and the edge of the cornea.

- Eyelashes are often present and introduce interference of a nature different to that offered by the eyelids. The eyelashes tend to produce outlying edges which can severely bias the fitting procedure if they are not accounted for.

- The transition from cornea to sclera is not sharp but is rather gradual. Therefore, traditional edge-detection techniques, such as Sobel filtering followed by thresholding, cannot be applied.

- The rings superimposed on the image in a placido disk-based videokeratoscope actually produce sharper edges than the limbus. The estimation algorithm must ignore these rings.

In this section, we present the proposed limbus estimation algorithm followed by a brief discussion.

### A. The Algorithm

A summary of the proposed corneal characterization algorithm, which has been formulated to accommodate the confounding factors listed above, is shown in Table I.

In the following, we describe in detail each of the steps of Table I using the image of the eye shown in Fig. 1 to illustrate the procedure. The image was obtained using the Optikon Keratron

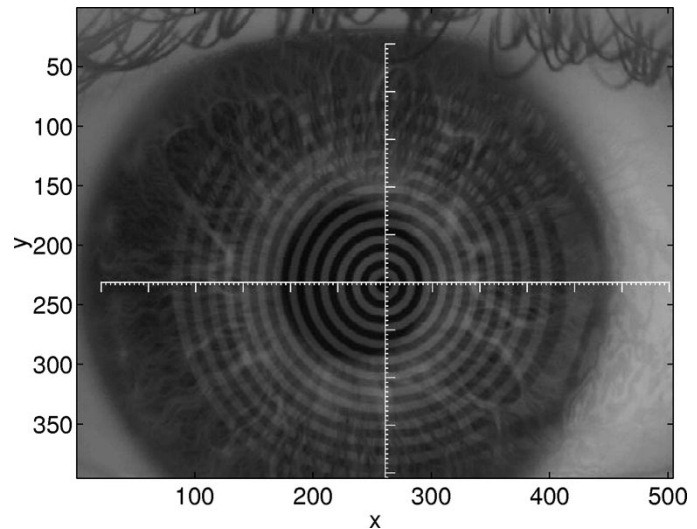


Fig. 1. Digital gray-scale image of the eye from a videokeratoscope with superimposed axis. The corneal vertex normal lies at the origin of the axis.

videokeratoscope. The eye shown in Fig. 1 has corneal astigmatism and exhibits all of the interferences mentioned above.

1) The vertex normal is the point at which the corneal surface is normal to the instrument axis and is located at the origin of the set of axes superimposed on the eye in the image of Fig. 1. To find the location of the corneal vertex normal we need to find the location of a white cross in the image. This can be easily achieved by using a cross mask (filter). Let  $c = h * g$  where  $*$  denotes the convolution operation and  $g(x, y)$  is an  $m \times m$  mask,  $m = 3, 5, \dots$ , defined as

$$g(x, y) = \begin{cases} 1, & x = (m+1)/2, y = 1, \dots, m; \\ & y = (m+1)/2, x = 1, \dots, m, \\ 0, & \text{otherwise.} \end{cases}$$

The convolved image  $c(x, y)$  will be maximized at the origin of the axes. Therefore, the position of the vertex normal is, in pixels

$$(x_n, y_n) = \arg \max_{x, y} c(x, y).$$

The location of the vertex normal will be used as an initial estimate of the location of the corneal centroid. The algorithm is not particularly sensitive to the size  $m$  of the mask, although it should be kept in mind that computational expense increases with  $m$ . In all of the examples presented in this paper, we use  $m = 21$  for the size of the mask.

Note that not all videokeratoscopes provide an image with a set of axes centered at the vertex normal. In such cases, the vertex normal can be found as the centroid of the innermost ring. Since finding the centroid of the innermost ring is not straightforward, an alternative may be to use  $(n_x/2, n_y/2)$  as the initial estimate of the corneal centroid. The rationale here is that the eye usually occupies an approximately central location in the image.

2) Set the initial value of the corneal centroid to  $(x_c^{(0)}, y_c^{(0)}) = (x_n, y_n)$  and initialize the counter variable  $d = 0$ .

3) While  $d < D$ , where  $D$  is the user-defined maximum number of iterations

a) Let  $\delta_r = r_{\max}/n_r$  be the radius step, where

$$r_{\max} = \max_{x,y} \sqrt{(x - x_c^{(d)})^2 + (y - y_c^{(d)})^2} / 40 + \epsilon, \quad (1)$$

$$\epsilon > 0$$

with  $(x_c^{(d)}, y_c^{(d)})$  being the estimate of the location of the corneal centroid at iteration  $d$ . Similarly, let  $\delta_\theta = 2\pi/n_\theta$  be the angular step. The quantity  $\epsilon$  is a small constant, say 0.01, chosen by the user and is included to ensure that

$$\sqrt{(x - x_c^{(d)})^2 + (y - y_c^{(d)})^2}$$

is strictly less than  $r_{\max}$  for  $x = 1, \dots, n_x, y = 1, \dots, n_y$ . The scaling factor of 1/40 converts from pixels to mm and will appear frequently. A  $n_r \times n_\theta$  polar grid may then be defined with pixel  $(i, j), i = 1, \dots, n_r, j = 1, \dots, n_\theta$  corresponding to radius  $r_i = (i - 1/2)\delta_r$  and angle  $\theta_j = (j - 1/2)\delta_\theta$ . An important consideration in this step is the choice of  $n_r$  and  $n_\theta$ , which are the dimensions of the polar grid. To avoid unnecessary computational expense, these integers should be chosen as small as possible without compromising accuracy.

b) Let  $h_p(i, j), i = 1, \dots, n_r, j = 1, \dots, n_\theta$  denote the image obtained by converting  $h(x, y)$  to polar coordinates. We form the image  $h_p(i, j)$  as follows. For  $x = 1, \dots, n_x, y = 1, \dots, n_y$ , set  $h_p(i, j) = h(x, y)$  where

$$i = \left\lfloor \sqrt{(x - x_c^{(d)})^2 + (y - y_c^{(d)})^2} / (40\delta_r) \right\rfloor + 1$$

$$j = \lfloor \{\psi(x, y) \bmod 2\pi\} / \delta_\theta \rfloor + 1$$

with  $\lfloor \cdot \rfloor$  denoting the floor operator, mod denoting the modulo operator and

$$\psi(x, y) = \arctan \left( \frac{y - y_c^{(d)}}{x - x_c^{(d)}} \right) + \begin{cases} 0, & x - x_c^{(d)} \geq 0 \\ \pi, & x - x_c^{(d)} < 0, y - y_c^{(d)} > 0 \\ -\pi, & x - x_c^{(d)} < 0, y - y_c^{(d)} < 0. \end{cases} \quad (2)$$

The operation described above assigns the image intensity value at Cartesian coordinates  $(x, y), x = 1, \dots, n_x, y = 1, \dots, n_y$  to the corresponding slot in the polar grid constructed in Step 3a). As will become apparent in later steps, the transformation from a Cartesian grid to a polar grid is performed to take advantage of the approximate circularity of the cornea. The result of transforming the image of Fig. 1 to a polar grid using  $n_r = 250, n_\theta = 180$ , and  $(x_n, y_n)$  as the center is shown in Fig. 2(a). Note that clockwise rotations are considered as positive when forming the digital image  $h_p(i, j)$ . To aid in the interpretation of this image a white line indicating the approximate position of the limbus, as selected manually, has been added. It can be seen that the limbus is quite far from being a straight line on the polar grid, as would be expected for a nearly circular object. This is due to the fact that, in this case, the corneal centroid is not close to the initial estimate which is given by the location of the vertex normal. In later iterations, when the corneal centroid estimate has been updated and is closer to the true value of the corneal centroid, the limbus will be an approximately straight line in

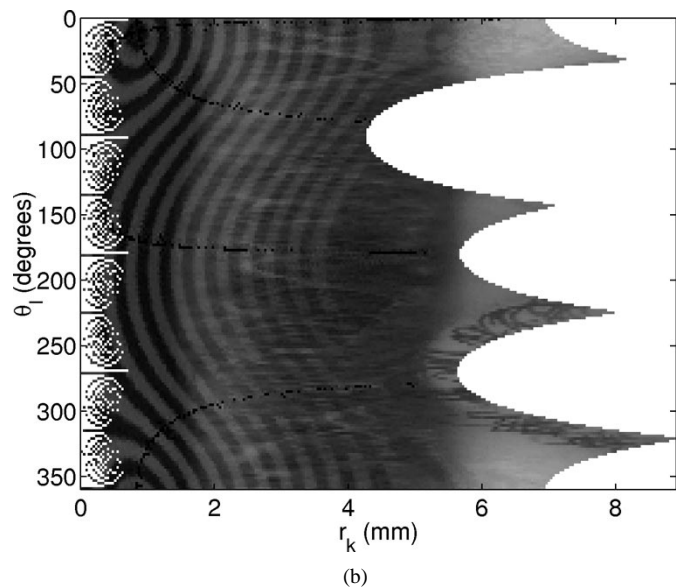
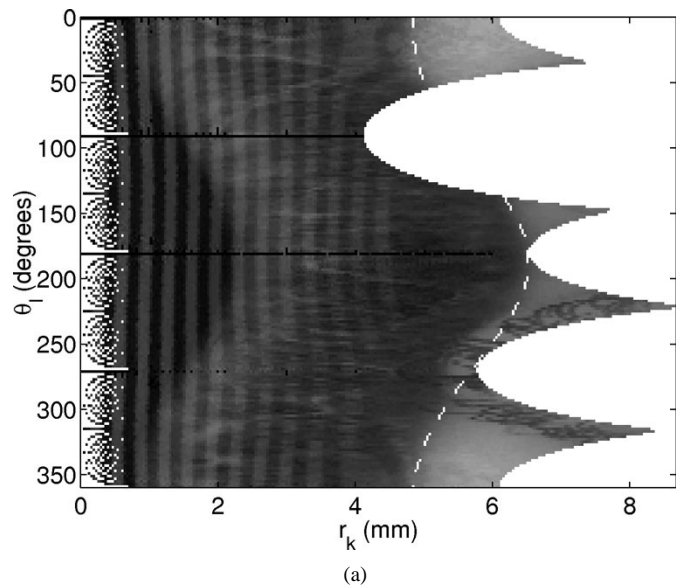


Fig. 2. Image of the eye converted to a polar grid using as the center (a) the location of the corneal vertex normal,  $(x_n, y_n)$ , and (b) the location estimated by the algorithm in the first iteration  $(x_c^{(1)}, y_c^{(1)})$ . A dashed white line indicating the approximate position of the limbus, as selected manually, is shown in (a).

the polar grid. This is shown in Fig. 2(b) where the corneal centroid estimate  $(x_c^{(1)}, y_c^{(1)})$  after the first iteration has been used to transform the image of Fig. 1 to a polar grid.

c) As mentioned previously, the transition from the cornea to the sclera is gradual and so cannot be detected using conventional edge-detection techniques. One option is to perform histogram equalization using three or four levels. The resulting image will have sharp edges at the limbus which can be detected using conventional techniques. However, we have found that this technique does not provide a sufficiently accurate edge. Specifically, the position of the edge depends heavily on the outcome of the histogram equalization which can sometimes result in significant errors. To obviate the need for histogram equalization we have developed the following procedure.

The presence of an edge is characterized by a large intensity-level gradient. In this case, we are searching for edges which

occur in the radial direction so we consider the gradient in the radial direction. The gradient in the radial direction at pixel  $(k, l)$  in the polar grid can be estimated by fitting a straight line to the intensity values  $h_p(i, l)$ ,  $i = k - \Delta, \dots, k + \Delta$  where  $\Delta$  is chosen so that the gradual edge presented by the limbus is accentuated and the sharp edges presented by the videokeratoscope rings are ignored. It is clear that a reasonably large value of  $\Delta$  is required since this will ensure that the cyclic changes in intensity produced by the videokeratoscope rings will have a small overall gradient and the gradual change produced by the limbus will have a large gradient. The estimation of the location of the limbus proceeds as follows. The radial gradient is computed for each pixel  $(k, l)$ ,  $k = \Delta + 1, \dots, n_r - \Delta$ ,  $l = 1, \dots, n_\theta$  and then, for each value of  $l$ , corresponding to angle  $\theta_l$ , the position of the limbus is taken as the location of the maximum gradient. Mathematically, let  $\gamma = (\gamma_0, \gamma_1)'$  be a two-element column vector containing the parameters of a local linear fit to the image intensities, and set

$$\hat{\gamma}(k, l) = \arg \min_{\gamma} \sum_{i=k-\Delta}^{k+\Delta} \{h_p(i, l) - (\gamma_0 + \gamma_1 r_i)\}^2 \quad (3)$$

for  $k = \Delta + 1, \dots, n_r - \Delta$ ,  $l = 1, \dots, n_\theta$  where  $\hat{\gamma}(k, l) = (\hat{\gamma}_0(k, l), \hat{\gamma}_1(k, l))'$  is a vector containing least squares estimators of the elements of  $\gamma$  at radius  $r_k$  and angle  $\theta_l$  and  $\Delta = \lfloor 3/(8\delta_r) + 1/2 \rfloor$ . The quantity  $\hat{\gamma}_1(k, l)$  is an estimate of the radial gradient at  $(k, l)$  and  $\hat{\gamma}_0(k, l)$  is a constant offset which, for our purposes, is a nuisance parameter which will be ignored. Note that  $2\Delta$  corresponds to a region which is 0.75 mm in length. A considerable saving in computation can be achieved by computing  $\hat{\gamma}(k, l)$  only for values of  $k$  at which the limbus may be reasonably supposed to exist. For example, assuming that the range of possible corneal diameters is 10–14 mm and that the magnitude of the difference between the corneal centroid estimate at iteration  $d$  and the true corneal centroid does not exceed  $\nu_d$  mm, we can restrict the computation of  $\hat{\gamma}(k, l)$  to  $k = \lfloor (5 - \nu_d)/\delta_r \rfloor, \dots, \min\{n_r - \Delta, \lfloor (7 + \nu_d)/\delta_r \rfloor\}$ .

The location of the edge at angle  $\theta_l$ ,  $l = 1, \dots, n_\theta$  is estimated as

$$\kappa(l) = \arg \max_k \hat{\gamma}_1(k, l)$$

which can be converted to millimeters to give  $\rho_l = r_{\kappa(l)}$ . Fitting straight lines to regions of length  $2\Delta$  means that sharp edges, such as those produced by the videokeratoscope rings or eyelashes, will be ignored, while the soft edge produced by the transition from the cornea to the sclera will be pronounced. In principle, the gradient of the straight line will be maximized at the mid-point of the transition from the cornea to the sclera. The edge estimation procedure is illustrated in Fig. 3 which shows  $h_p(k, 165)$  [Fig. 3(a)] and  $\hat{\gamma}_1(k, 165)$  [Fig. 3(b)] plotted against  $r_k$ . Clearly, the peak of  $\hat{\gamma}_1(k, 165)$  occurs at a point which is roughly at the mid-point of the transition.

d) The procedure of Step 3c) is not infallible and sometimes results in the appearance of false edges due to eyelashes and eyelids. The videokeratoscope rings also produce false edges in semi-meridians where the eye is not completely in picture, such as  $70 < \theta_l < 110$  for the image of Fig. 1. These interferences may be removed or reduced by taking advantage of the approx-

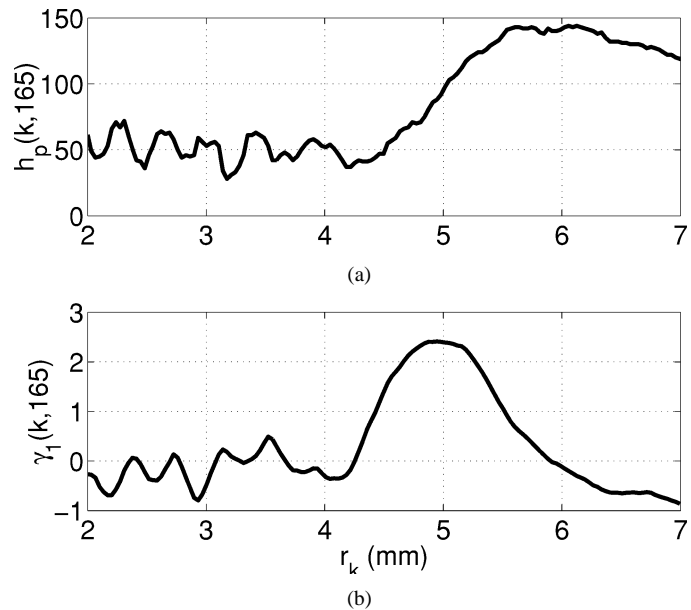


Fig. 3. Plots of the intensity profile of (a), the digital image  $h_p(k, 165)$  and (b) the intensity gradient  $\hat{\gamma}_1(k, 165)$  against  $r_k$  (in mm).

imate circularity of the limbus. When the estimate  $(x_c^{(d)}, y_c^{(d)})$  of the corneal centroid is close to the true value of the corneal centroid, the limbus will be an approximately vertical line on the polar grid. Therefore, the edge points  $\rho_l$ ,  $l = 1, \dots, n_\theta$  found in Step 3c) which are due to the limbus should be restricted to a narrow range of values. Steps 3d) and e) aim to use this property to remove edge points which are not due to the limbus. In Step 3d), we find the maximum value  $R$  of  $\rho_l$ ,  $l = 1, \dots, n_\theta$  which can be considered to be part of the limbus. This is done by finding the largest value of  $\rho_k$  for which the percentage of values of  $\rho_l \in [\rho_k - \tau_d, \rho_k]$  exceeds  $n_\theta \lambda_d$  where  $\tau_d$  and  $\lambda_d$  are parameters given below. To express this idea mathematically we define the indicator function

$$I_{[r-\tau_d, r]}(\rho_j) = \begin{cases} 1, & \rho_j \in [r - \tau_d, r] \\ 0, & \text{otherwise} \end{cases}$$

where  $\tau_d = 0.3$  for  $d \leq 1$  and 0.1 for  $d > 1$  and let  $R$  be the largest value of  $\rho_l$  for which

$$\sum_{j=1}^{n_\theta} I_{[\rho_l - \tau_d, \rho_l]}(\rho_j) > n_\theta \lambda_d$$

where  $\lambda_d = 1/20$  for  $d = 0$  and  $1/10$  for  $d > 0$ .

e) In this step, we aim to remove from consideration edge points at radii beyond the limbus, which are often due to eyelashes, and edge points at radii less than the limbus, which are due to the videokeratoscope rings and the eyelids. Specifically, we consider the edge points  $\rho_l$  such that  $l \in \Theta$  where  $\Theta = \{l \in \{1, \dots, n_\theta\} | R - \xi_d \leq \rho_l \leq R\}$  where

$$\xi_d = \begin{cases} 2, & d = 0 \\ 0.75, & d = 1 \\ 0.3, & d = 2. \end{cases}$$

Note that the requirements imposed by the parameters  $\tau_d$ ,  $\lambda_d$ , and  $\xi_d$  become stricter as the iteration number  $d$  increases. The reason for this becomes apparent upon inspection of images in Fig. 2. In the initial iteration, it cannot be assumed that the limbus will be approximately vertical so the rejection of

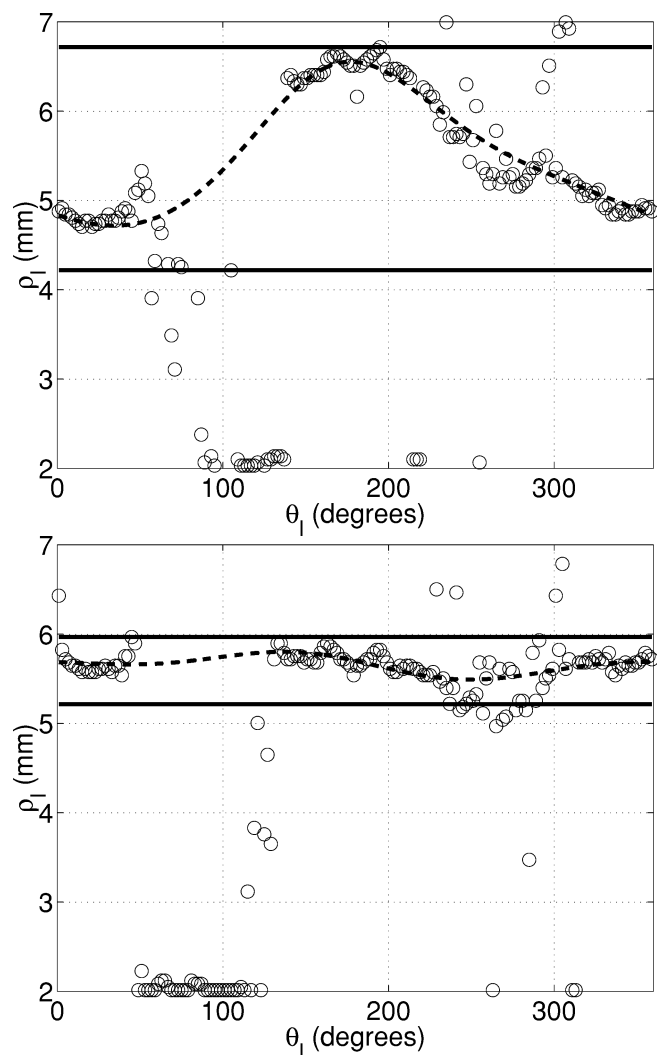


Fig. 4. Plot of the estimated edge location  $\rho_l$  (“o”) against  $\theta_l$  (in degrees) for (a) the first iteration and (b) the second iteration. The range of values of  $\rho_l$  used in the ellipse fit is indicated by solid lines and the ellipse fit is indicated by a dashed line.

edge points must be done with care. After the first iteration, the corneal centroid estimate is sufficiently accurate that the limbus will be approximately vertical on a polar grid so stricter conditions can be used to remove false edge points without also removing edge points due to the limbus. The procedure is illustrated in Fig. 4 which shows plots of  $\rho_l$  against  $\theta_l$  for the first and second iterations. The resulting elliptical fit for each iteration is indicated by a dashed line. Values of  $\rho_l$  which fall between the two horizontal solid lines marked on the graphs are taken as limbus edges and are used in subsequent calculations. It can be seen that, in the second iteration, a much tighter range can be used thus allowing most of the eyelid edge points to be omitted. This is clearly not possible in the first iteration due to the wide variation of the limbus edge points.

f) Fit an ellipse to  $\rho_l$ ,  $l \in \Theta$  by minimizing the algebraic distance in the least-squares sense

$$\left( \hat{x}_0, \hat{y}_0, \hat{a}, \hat{b}, \hat{\phi} \right) = \arg \min_{x_0, y_0, a, b, \phi} \sum_{l \in \Theta} q(\rho_l, \theta_l; x_0, y_0, a, b, \phi)^2 \quad (4)$$

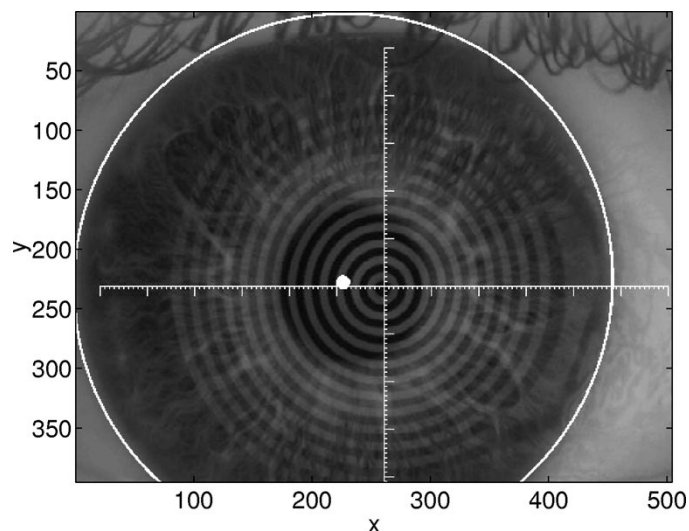


Fig. 5. Image of Fig. 1 with elliptical fit superimposed. The estimated location of the corneal centroid is indicated by a white dot.

where  $q(r, \theta; x_0, y_0, a, b, \phi) = 0$  is the equation of an ellipse centered at  $(x_0, y_0)$  with angular rotation  $\phi$  and axis length  $2a$  in the  $\phi$  direction and axis length  $2b$  in the  $\phi + \pi/2$  direction,

$$\begin{aligned} q(r, \theta; x_0, y_0, a, b, \phi) &= \{r \cos(\theta) - x_0\}^2 \zeta_1(p, \phi) \\ &+ 2\{r \cos(\theta) - x_0\} \{r \sin(\theta) - y_0\} \zeta_2(p, \phi) \\ &+ \{r \sin(\theta) - y_0\}^2 \zeta_3(p, \phi) - b^2 = 0 \end{aligned} \quad (5)$$

with

$$\zeta_1(p, \phi) = p \cos^2(\phi) + \sin^2(\phi) \quad (6)$$

$$\zeta_2(p, \phi) = \cos(\phi) \sin(\phi) (1 - p) \quad (7)$$

$$\zeta_3(p, \phi) = p \sin^2(\phi) + \cos^2(\phi) \quad (8)$$

and  $p = b^2/a^2$  (see the Appendix).

g) Set  $x_c^{(d+1)} = x_c^{(d)} + 40\hat{x}_0$ ,  $y_c^{(d+1)} = y_c^{(d)} + 40\hat{y}_0$ , where the scale factor of 40 converts from mm to pixels, and increment  $d$ .

An ellipse is fitted to the accepted edge points  $\rho_l$ ,  $l \in \Theta$  by minimizing the sum of the squared algebraic errors. Some manipulations are required in order to frame (4) as a linear least squares problem. The approach we have used is given in the Appendix. Although more robust techniques may be employed to fit an ellipse to data [16], [17], the chosen method is computationally efficient and is sufficiently robust for our purposes, particularly after outliers have been removed in the manner described above.

After the current corneal centroid estimates have been updated the counter variable  $d$  is incremented, steps 3a)–3g) are repeated if  $d < D$ . Otherwise, the modeling procedure is complete and the parameters of the elliptical fit,  $\hat{x}_c = (x_c^{(D)} - x_n)/40$ ,  $\hat{y}_c = (y_c^{(D)} - y_n)/40$ ,  $\hat{a}$ ,  $\hat{b}$  and  $\hat{\phi}$ , where distances are in mm, provide a parametric 2-D characterization of the cornea. Note that the coordinates of the corneal centroid are defined relative to the vertex normal provided by the videokeratoscope. In Fig. 5, the image of Fig. 1 has been superimposed with a white line indicating the final elliptical fit and a white dot located at the corneal centroid. Clearly, the procedure has managed to provide an accurate fit to the limbus despite the numerous inter-

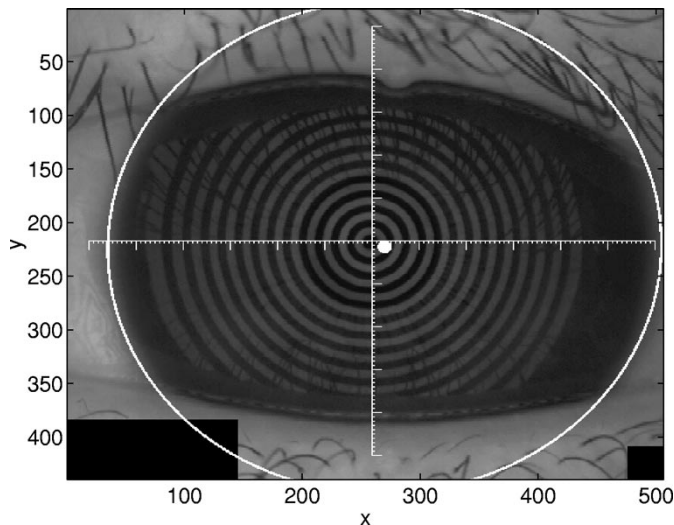


Fig. 6. Image of an eye with the cornea obstructed by the eyelids. The elliptical fit found by the proposed algorithm is superimposed. The estimated location of the corneal centroid is indicated by a white dot.

ferences present in the image. An additional example in which the cornea is severely obstructed by the eyelids is included to demonstrate the performance of the algorithm in adverse conditions. The image of the eye superimposed with a white line indicating the elliptical fit is shown in Fig. 6. A good fit has been obtained despite the fact that a large portion of the cornea is not visible.

### B. Discussion

The design of the proposed algorithm required the selection of various parameters, namely  $\tau_d$ ,  $\lambda_d$  and  $\xi_d$  of steps 3d) and e), using a representative set of training images. The empirical nature of this process does not preclude the possibility of encountering an image which the algorithm cannot handle. However, we have endeavored to minimize the occurrence of such an event by trialing the algorithm on a large number of images exhibiting all possible types and degrees of interference using the selected parameters. Satisfactory results have been obtained in all cases. The examples given in this section clearly indicate the robustness of the proposed algorithm, and therefore the suitability of the chosen parameters. The first example contains a significantly decentered vertex normal as well as obstruction due to the eyelids and interference from eyelashes. In the second example a large portion of the limbus is not visible due to obstruction by the eyelids. It may be appreciated that the vast majority of images are of far better quality than these two images.

The proposed algorithm has been implemented in Matlab. With the number of iterations set to three, the algorithm takes 90 seconds to run on a Pentium IV 1.8-GHz computer. The Matlab code is available from the authors upon request.

## III. EXPERIMENTAL RESULTS

In this section, we assess the corneal characterization algorithm of the previous section using a data set of the left and right eyes of 16 subjects. The group contained subjects

from a variety of ethnic backgrounds, resulting in a mix of iris pigmentation and eyelid characteristics. Nine of the subjects had corneal with-the-rule astigmatism meaning that the flattest meridian is within  $20^\circ$  of horizontal. Three of the subjects had corneal against-the-rule astigmatism (flattest meridian within  $20^\circ$  of vertical) and two subjects had oblique astigmatism, i.e., neither with- or against-the-rule. The remaining two subjects had a pathological condition known as keratoconus resulting in inferior corneal steepening.

A manual method of performing 2-D characterization of the cornea is required in order to provide a basis for comparison with the proposed algorithm. One manual method which we have used is to produce a series of concentric circles on a transparency. This transparency is then overlaid on the corneal image and manually aligned to give a best fit to the corneal limbus. This method is not suitable for our purposes because it provides information only about the corneal centroid and does not perform well for corneas whose shape deviates significantly from circularity. To overcome these problems the following computer-based manual technique has been developed.

Given an image of the eye the operator uses a mouse to select  $n$  evenly spaced points,  $(r_1, \theta_1), \dots, (r_n, \theta_n)$ ,  $n \geq 5$ , which are deemed to lie on the limbus. The polar coordinates are defined with respect to the location  $(x_n, y_n)$  of the vertex normal, as found in Step 1 in Table I. An ellipse is fitted to the selected points by minimizing the sum of squared algebraic errors

$$(\tilde{x}_c, \tilde{y}_c, \tilde{a}, \tilde{b}, \tilde{\phi}) = \arg \min_{x_0, y_0, a, b, \phi} \sum_{i=1}^n q(r_i, \theta_i; x_0, y_0, a, b, \phi)^2$$

where  $q(r, \theta; x_0, y_0, a, b, \phi)$  is given in (5). The parameters  $\tilde{x}_c$  and  $\tilde{y}_c$  are estimates of the location of the corneal centroid relative to the vertex normal. In order to reduce the effects of operator bias, we combine measurements from several operators to obtain

$$(\tilde{x}_c, \tilde{y}_c, \tilde{a}, \tilde{b}, \tilde{\phi}) = \arg \min_{x_0, y_0, a, b, \phi} J(x_0, y_0, a, b, \phi)$$

where

$$J(x_0, y_0, a, b, \phi) = \sum_{j=1}^p \sum_{i=1}^n q(r_{i,j}, \theta_{i,j}; x_0, y_0, a, b, \phi)^2$$

with  $(r_{i,j}, \theta_{i,j})$  denoting the  $i$ th point selected by the  $j$ th operator,  $j = 1, \dots, p$ . Despite the presence of operator bias, which is reduced through the use of multiple operators, the estimates  $\tilde{x}_c$ ,  $\tilde{y}_c$ ,  $\tilde{a}$ ,  $\tilde{b}$ , and  $\tilde{\phi}$  may be regarded as providing an accurate corneal characterization which will be used as a benchmark for assessing the proposed algorithm. In the following, we use  $n = 16$  points and  $p = 3$  operators and the dimensions of the polar grid used in the algorithm of Section II are  $n_r = 250$  and  $n_\theta = 180$  and the number of iterations is set to  $D = 3$ .

We begin by examining the differences between the overall fits obtained by the manual computer-based method and the algorithm. As a measure of the differences between two fits we use the root-mean-square (RMS) difference between the distances from the vertex normal to the fitted ellipse at each semi-

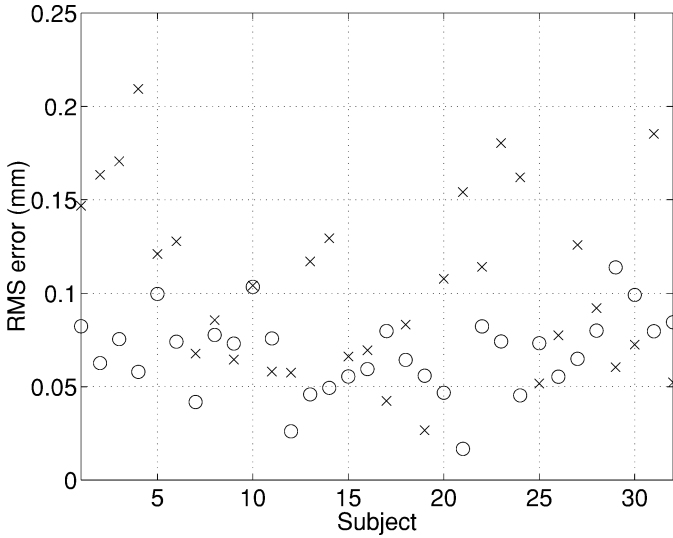


Fig. 7. RMS error (in millimeters) between the limbus fits for the manual computer-based method and the proposed algorithm (“o”) and an algorithm which uses histogram equalization and Sobel filtering for edge detection (“x”).

meridian. The RMS difference between the proposed algorithm and the manual technique is

$$\sqrt{\frac{1}{l} \sum_{i=1}^l \left\{ r_e(\theta_i; \hat{x}_c, \hat{y}_c, \hat{a}, \hat{b}, \hat{\phi}) - r_e(\theta_i; \tilde{x}_c, \tilde{y}_c, \tilde{a}, \tilde{b}, \tilde{\phi}) \right\}^2} \quad (9)$$

where  $\theta_i = 2\pi(i-1)/l$ ,  $i = 1, \dots, l$  and

$$r_e(\theta; x_0, y_0, a, b, \phi) = \left( -c_1 \pm \sqrt{c_1^2 - 4c_2c_0} \right) / (2c_2)$$

where

$$\begin{aligned} c_0 &= x_0^2 \zeta_1(p, \phi) + 2x_0y_0 \zeta_2(p, \phi) + y_0^2 \zeta_3(p, \phi) - b^2 \\ c_1 &= -2[\cos(\theta)\{x_0 \zeta_1(p, \phi) + y_0 \zeta_2(p, \phi)\} \\ &\quad + \sin(\theta)\{y_0 \zeta_3(p, \phi) + x_0 \zeta_2(p, \phi)\}] \\ c_2 &= \cos^2(\theta) \zeta_1(p, \phi) + 2\cos(\theta)\sin(\theta) \zeta_2(p, \phi) \\ &\quad + \sin^2(\theta) \zeta_3(p, \phi) \end{aligned}$$

with  $\zeta_i(p, \phi)$ ,  $i = 1, 2, 3$  defined in (6)–(8) and  $p = b^2/a^2$ .

The main computational expense of the proposed algorithm is incurred during the edge-detection step which requires  $(n_r - 2\Delta) \cdot n_\theta$ , where  $\Delta$  is typically about  $n_r/10$ , first-order polynomial fits for an  $n_r \times n_\theta$  polar grid. In the interest of reducing the computational burden imposed by this edge-detection procedure, it is desirable to consider alternative methods. One possibility, which makes use of conventional image processing techniques, is to perform histogram equalization followed by Sobel filtering and thresholding. The validity of this approach, to be referred to as the alternative algorithm, will be assessed in this section. We will refer to the procedure described in Section II as the proposed algorithm. Parameter estimates obtained by the alternative algorithm are denoted as  $\tilde{x}_c$ ,  $\tilde{y}_c$ ,  $\tilde{a}$ ,  $\tilde{b}$ , and  $\tilde{\phi}$ .

The RMS difference between the manual technique and the alternative algorithm is defined as in (9) with  $\hat{x}_c$ ,  $\hat{y}_c$ ,  $\hat{a}$ ,  $\hat{b}$ , and  $\hat{\phi}$  replaced by  $\tilde{x}_c$ ,  $\tilde{y}_c$ ,  $\tilde{a}$ ,  $\tilde{b}$ , and  $\tilde{\phi}$ . In the following, we set  $l = 720$  in (9). Fig. 7 shows the RMS differences between the manual technique and both algorithms for each subject. It can be seen that the RMS difference between the proposed algorithm and

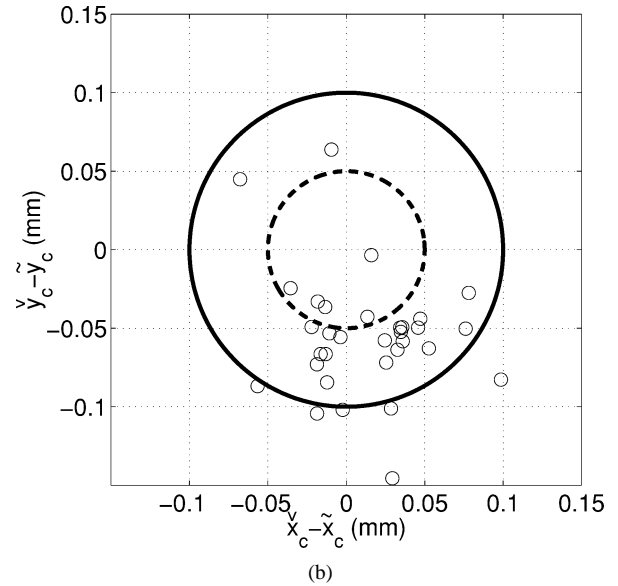
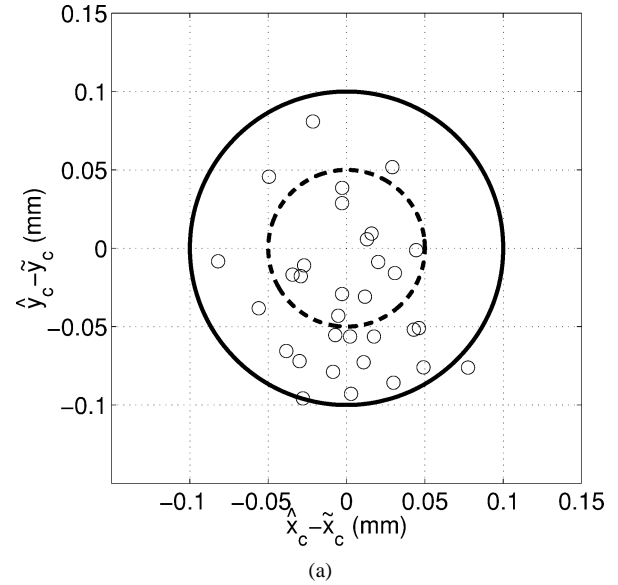


Fig. 8. Centroid differences between the manual computer-based method and (a) the proposed algorithm and (b) an algorithm which uses histogram equalization and Sobel filtering for edge detection. Circles of radius 0.1 mm (solid) and 0.05 mm (dashed) are shown.

the manual technique does not exceed 0.12 mm for any subject. The alternative algorithm is clearly less accurate in most cases with RMS differences as large as 0.21 mm. The RMS difference between the proposed algorithm and the manual technique is less than the RMS difference between the alternative algorithm and the manual technique in 24 cases out of 32.

It is also of interest to examine the differences between the corneal centroid estimates as these parameters are of particular interest in various clinical applications. Fig. 8 shows  $\hat{y}_c - \tilde{y}_c$  plotted against  $\hat{x}_c - \tilde{x}_c$  and  $\hat{y}_c - \tilde{y}_c$  plotted against  $\hat{x}_c - \tilde{x}_c$  for each subject. Circles enclosing points with an absolute value less than 0.1 mm (solid) and 0.05 mm (dashed) are shown. It can be seen that absolute value of the difference between the centroid estimates of the proposed algorithm and the manual technique exceeds 0.1 mm for only one subject. In 13 cases, the absolute value of the difference is less than 0.05 mm. The alternative algorithm is considerably less accurate with absolute

differences greater than 0.1 mm for six subjects and absolute differences of less than 0.05 mm for only five subjects.

It can be seen from Fig. 8 that there is a tendency for the  $y$  coordinate of the centroid estimates obtained from the computer algorithms to be smaller than that obtained from the manual technique, particularly in the case of the alternative algorithm. To investigate the possibility of a bias, we have performed two-sample  $t$ -tests for the difference between the means of the  $y$  coordinates of the centroids returned by the automatic algorithms and the manual algorithm. The tests returned  $p$ -values of 0.332 for the difference between the proposed algorithm and the manual algorithm and 0.084 for the difference between the alternative algorithm and the manual algorithm. Therefore neither algorithm shows a significant bias with respect to the manual algorithm at the 5% level although the possibility of a bias between the alternative algorithm and the manual technique cannot be discarded entirely.

The veracity of the proposed algorithm for automated 2-D corneal characterization is demonstrated by the results of this section which show a close agreement between the proposed algorithm and a reliable benchmark supplied by a manual computer-based method. An alternative algorithm which eschews the computationally expensive edge-detection algorithm in Step 3c) in favor of conventional image processing techniques proved to be less accurate in most cases. A certain degree of caution is required when interpreting the results of this section, since comparisons such as those illustrated in Figs. 7 and 8 are a reflection of the relative accuracy of the two algorithms only to the extent that the manual technique supplies accurate estimates of the limbus. It seems reasonable to assume as much since the main source of error in the manual technique is operator bias which has been greatly reduced by the use of multiple operators.

#### IV. CONCLUSION

An accurate and robust method for estimating the corneal limbus in videokeratographic images has been proposed. It has been shown that the proposed estimation algorithm outperforms traditional edge-detection techniques based on histogram equalization and Sobel filtering. A comparison with manual estimation of the limbus indicates that the algorithm closely mimics the actions of an advanced human operator. This makes it a valuable tool in videokeratography. The edge-detection procedure proposed in this paper is more computationally demanding than the traditional approaches due to the large number of first-order polynomial fits required. However, in an era of exponentially increasing computational power this should not be an obstacle in adapting the algorithm into commercial instruments. It is anticipated that the proposed corneal limbus estimation algorithm can be also adapted for estimation of the pupil perimeter.

#### APPENDIX

##### LEAST SQUARES ESTIMATION OF THE ELLIPSE PARAMETERS

In this appendix, the least-squares procedure used to estimate the parameters of the ellipse fitted to the limbus is described. It is assumed that  $n$  data points  $(r_1, \theta_1), \dots, (r_n, \theta_n)$  are available from which the ellipse parameters are to be estimated.

An ellipse centered at  $(x_0, y_0)$  with axes lengths  $2a$  and  $2b$  in the  $x$  and  $y$  directions, respectively, has the equation

$$(x - x_0)^2/a^2 + (y - y_0)^2/b^2 = 1.$$

Rotating the ellipse by an angle  $\phi$  results in the equation

$$p\{(x - x_0)\cos(\phi) + (y - y_0)\sin(\phi)\}^2 + \{(y - y_0)\cos(\phi) - (x - x_0)\sin(\phi)\}^2 = b^2$$

where  $p = b^2/a^2$ . Substituting  $x = r\cos(\theta)$  and  $y = r\sin(\theta)$  and performing some straightforward manipulations yields

$$\{r\cos(\theta) - x_0\}^2\zeta_1(p, \phi) + \{r\sin(\theta) - y_0\}^2\zeta_3(p, \phi) + 2\{r\cos(\theta) - x_0\}\{r\sin(\theta) - y_0\}\zeta_2(p, \phi) - b^2 = 0 \quad (10)$$

where  $\zeta_i(p, \phi)$ ,  $i = 1, 2, 3$  are given in (6)–(8).

Expanding the brackets in (10) and grouping terms gives

$$\begin{aligned} & r^2\cos^2(\theta)\zeta_1(p, \phi) + r^2\sin^2(\theta)\zeta_3(p, \phi) \\ & + 2r^2\cos(\theta)\sin(\theta)\zeta_2(p, \phi) \\ & - 2r\cos(\theta)\{x_0\zeta_1(p, \phi) + y_0\zeta_2(p, \phi)\} \\ & - 2r\sin(\theta)\{y_0\zeta_3(p, \phi) + x_0\zeta_2(p, \phi)\} \\ & + x_0^2\zeta_1(p, \phi) + 2x_0y_0\zeta_2(p, \phi) + y_0^2\zeta_3(p, \phi) - b^2 = 0. \end{aligned} \quad (11)$$

Errors in the edge-detection algorithm and model mis-match between the ellipse and the actual limbus shape result in the existence of noise in the observations  $(r_1, \theta_1), \dots, (r_n, \theta_n)$ . We, therefore, obtain

$$\mathbf{z} = \mathbf{H}\boldsymbol{\alpha} + \boldsymbol{\epsilon}$$

where  $\mathbf{z} = (r_1^2\cos^2(\theta_1), \dots, r_n^2\cos^2(\theta_n))'$ ,  $\boldsymbol{\epsilon} = (\epsilon_1, \dots, \epsilon_n)'$  is a vector of disturbances which we assume to be random and uncorrelated

$$\mathbf{H} = \begin{pmatrix} -2r_1^2\cos(\theta_1)\sin(\theta_1) & \cdots & -2r_n^2\cos(\theta_n)\sin(\theta_n) \\ -r_1^2\sin^2(\theta_1) & \cdots & -r_n^2\sin^2(\theta_n) \\ 2r_1\cos(\theta_1) & \cdots & 2r_n\cos(\theta_n) \\ 2r_1\sin(\theta_1) & \cdots & 2r_n\sin(\theta_n) \\ -1 & \cdots & -1 \end{pmatrix}'$$

and  $\boldsymbol{\alpha} = (\alpha_1, \dots, \alpha_5)'$  where

$$\alpha_1 = \zeta_2(p, \phi)/\zeta_1(p, \phi) \quad (12)$$

$$\alpha_2 = \zeta_3(p, \phi)/\zeta_1(p, \phi) \quad (13)$$

$$\alpha_3 = x_0 + y_0\zeta_2(p, \phi)/\zeta_1(p, \phi) \quad (14)$$

$$\alpha_4 = \{y_0\zeta_3(p, \phi) + x_0\zeta_2(p, \phi)\}/\zeta_1(p, \phi) \quad (15)$$

$$\alpha_5 = x_0^2 + \{2x_0y_0\zeta_2(p, \phi) + y_0^2\zeta_3(p, \phi) - b^2\}/\zeta_1(p, \phi). \quad (16)$$

The estimate of the parameter vector  $\boldsymbol{\alpha}$  which minimizes the sum of squared arithmetic errors  $(\mathbf{z} - \mathbf{H}\boldsymbol{\alpha})'(\mathbf{z} - \mathbf{H}\boldsymbol{\alpha})$  is

$$\hat{\boldsymbol{\alpha}} = (\mathbf{H}'\mathbf{H})^{-1}\mathbf{H}'\mathbf{z}.$$

Since we would like estimates of  $x_0$ ,  $y_0$ ,  $a$ ,  $b$ , and  $\phi$  we must transform the elements of  $\hat{\boldsymbol{\alpha}}$  using (12)–(16). Note that the estimates obtained from transforming the elements of  $\hat{\boldsymbol{\alpha}}$  also minimize the sum of the squared algebraic errors. In the following, the parameters in (12)–(16) are replaced by their least-squares estimates. Rearranging (13) gives

$$\hat{p} = \left\{ 1 - \hat{\alpha}_2 \tan^2(\hat{\phi}) \right\} / \left\{ \hat{\alpha}_2 - \tan^2(\hat{\phi}) \right\}. \quad (17)$$



Substituting (17) into (12) and performing some straightforward manipulations gives

$$\hat{\alpha}_1 = \tan(\hat{\phi}) (1 - \hat{\alpha}_2) / \{1 - \tan^2(\hat{\phi})\}.$$

From the resulting quadratic in  $\tan(\hat{\phi})$  we obtain the following equation for  $\hat{\phi}$ :

$$\hat{\phi} = \arctan\left(\frac{\hat{\alpha}_2 - 1 \pm \sqrt{(1 - \hat{\alpha}_2)^2 + 4\hat{\alpha}_1^2}}{2\hat{\alpha}_1}\right). \quad (18)$$

The choice between  $\pm$  in (18) is arbitrary. The estimate  $\hat{p}$  of  $p$  is found by substituting  $\hat{\phi}$  and  $\hat{\alpha}_2$  into (17).

Rearranging (14) gives

$$\hat{x}_0 = \hat{\alpha}_3 - \hat{y}_0 \zeta_2(\hat{p}, \hat{\phi}) / \zeta_3(\hat{p}, \hat{\phi}). \quad (19)$$

Substituting (19) into (15) and rearranging gives

$$\hat{y}_0 = \left\{ \zeta_1(\hat{p}, \hat{\phi}) \hat{\alpha}_4 - \zeta_2(\hat{p}, \hat{\phi}) \hat{\alpha}_3 \right\} / \left\{ \zeta_3(\hat{p}, \hat{\phi}) - \zeta_2^2(\hat{p}, \hat{\phi}) / \zeta_3(\hat{p}, \hat{\phi}) \right\}.$$

The estimate store  $\hat{x}_0$  of  $x_0$  is found by substituting  $\hat{y}_0$ ,  $\hat{p}$ ,  $\hat{\phi}$  and  $\hat{\alpha}_3$  into (19). The estimate  $\hat{b}$  of  $b$  can be found using (16) as

$$\hat{b} = \sqrt{\zeta_1(\hat{p}, \hat{\phi}) (\hat{x}_0^2 - \hat{\alpha}_5) + 2\hat{x}_0 \hat{y}_0 \zeta_2(\hat{p}, \hat{\phi}) + \hat{y}_0^2 \zeta_3(\hat{p}, \hat{\phi})}.$$

Finally,  $\hat{a} = \hat{b} / \sqrt{\hat{p}}$ .

REFERENCES

[1] P. M. Kiely, G. Smith, and L. G. Carney, "The mean shape of the human cornea," *Optica Acta*, vol. 29, no. 8, pp. 1027–1040, 1982.  
 [2] R. A. Applegate and H. C. Howland, "Noninvasive measurement of corneal topography," *IEEE Eng. Med. Biol. Mag.*, vol. 14, no. 1, pp. 30–42, 1995.  
 [3] R. B. Mandell, "A guide to videokeratography," *Int. Contact Lens Clinic*, vol. 23, no. 6, pp. 205–228, 1996.  
 [4] C. Roberts, "Corneal topography: A review of terms and concepts," *J. Cataract Refract. Surg.*, vol. 23, pp. 624–629, 1996.  
 [5] R. Mattioli and N. K. Tripoli, "Corneal geometry reconstruction with the Keratron videokeratograph," *Optom. Vis. Sci.*, vol. 74, no. 11, pp. 881–894, 1997.  
 [6] D. Brenner, "Modeling the cornea with the topographic modeling system videokeratoscope," *Optom. Vis. Sci.*, vol. 74, no. 11, pp. 895–898, 1997.  
 [7] C. Campbell, "Reconstruction of the corneal shape with the MasterVue corneal topography system," *Optom. Vis. Sci.*, vol. 74, no. 11, pp. 899–905, 1997.  
 [8] D. R. Iskander, M. J. Collins, and B. Davis, "Optimal modeling of corneal surfaces with Zernike polynomials," *IEEE Trans. Biomed. Eng.*, vol. 48, pp. 87–95, Jan. 2001.  
 [9] D. R. Iskander, M. R. Morelande, M. J. Collins, and B. Davis, "Modeling of corneal surfaces with radial polynomials," *IEEE Trans. Biomed. Eng.*, vol. 49, pp. 320–328, Apr. 2002.  
 [10] I. Karpouzias and Y. Pouliquen, "Modeling and numerical optimization of corneal rotation," *IMA J. Math. Appl. Med. Biol.*, vol. 8, pp. 73–82, 1991.  
 [11] A. Langenbacher, B. Seitz, M. M. Kus, E. Vilchis, and G. O. Naumann, "Graft decentration in penetrating keratoplasty: Nonmechanical trephination with the excimer laser (193 nm) versus the motor trephine," *Ophthalm. Surg. Lasers*, vol. 29, no. 2, pp. 106–113, 1998.  
 [12] R. B. Mandell, C. S. Chiang, and S. A. Klein, "Location of major corneal reference points," *Optom. Vis. Sci.*, vol. 72, no. 11, pp. 776–784, 1995.  
 [13] J. Schwiagerling and R. W. Snyder, "Eye movement during laser *in situ* keratomileusis," *J. Cataract Refract. Surg.*, vol. 26, no. 3, pp. 345–351, 2000.  
 [14] D. K. Martin and B. A. Holden, "A new method for measuring the diameter of the *in vivo* human cornea," *Amer. J. Optomet. Physiol. Optics*, vol. 59, no. 5, pp. 436–441, 1982.

[15] I. Karpouzias and Y. Pouliquen, "Computerized method for rotational autokeratoplasty," *Cornea*, vol. 10, no. 5, pp. 369–371, 1991.  
 [16] J. Cabrera and P. Meer, "Unbiased estimation of ellipse by bootstrapping," *IEEE Trans. Pattern Anal. Machine Intell.*, vol. 18, pp. 752–756, July 1996.  
 [17] Z. Zhang, "Parameter estimation techniques: A tutorial with application to conic fitting," *Image Vis. Computing*, vol. 15, pp. 59–76, 1997.



**Mark R. Morelande** received the B.Eng. degree in aerospace avionics from Queensland University of Technology, Brisbane, Australia, in 1997 and the Ph.D. degree in electrical engineering from Curtin University of Technology, Perth, Australia, in 2001.

From November 2000–January 2002 he was a Postdoctoral Fellow at the Centre for Eye Research, Queensland University of Technology. Since January 2002, he has been a Research Fellow at the Cooperative Research Centre for Sensor, Signal and Information Processing, University of Melbourne.

His research interests lie in the area of statistical signal processing, in particular nonstationary signal analysis and target tracking.



**D. Robert Iskander** (M'98) received the Magister Inżynier degree in electronic engineering from the Technical University of Lodz, Poland, in 1991, and the Ph.D. degree in signal processing from Queensland University of Technology (QUT), Australia, in 1997. From 1996 to 2000, he was a Research Fellow at the Signal Processing Research Centre, the Cooperative Research Centre for Satellite Systems, and the Centre for Eye Research, QUT. In 2001, he joined the School of Engineering, Griffith University, Australia, as a Senior Lecturer. He is also a Visiting Research

Fellow at the Centre for Eye Research, QUT, and an Associate Member of the Communications and Signal Processing Group at Curtin University of Technology, Perth, Australia. His current research interests include statistical signal processing, visual optics, and optometry.

Dr. Iskander is a member of the Association for Research in Vision and Ophthalmology.



**Michael J. Collins** received the Dip.App.Sc. (optom), M.App.Sc., and Ph.D. degrees from Queensland University of Technology, Brisbane, Australia, in 1977, 1988, and 1996, respectively.

He is an Associate Professor in the School of Optometry at the Queensland University of Technology. His research laboratory, the Contact Lens and Visual Optics Laboratory, specializes in the visual and optical characteristics of the cornea and contact lenses.

Dr. Collins is a member of the Optometrists Association of Australia, Fellow of the American Academy of Optometry, a Fellow of the Contact Lens Society of Australia, and a member of the International Society for Contact Lens Research.



**Ross Franklin** received the Bachelor of Applied Science B.App.Sc. degree in optometry from the Queensland University of Technology in 1991.

He worked in private practice until 1998, when he began work as a research optometrist at the Contact Lens and Visual Optics Laboratory, QUT. His chief research interests are corneal topography, contact lenses, and wavefront aberrations.